Abstract spaces, mappings and geometry in the study of optical systems

Miguel Alonso

Abstract spaces, mappings and geometry in the study of optical systems

Miguel A. Alonso*
Aix Marseille Univ., CNRS, Centrale Marseille, Institut Fresnel, UMR 7249, 13397 Marseille Cedex 20, France; The Institute of Optics and Center for Freeform Optics, University of Rochester, Rochester NY 14627, U.S.A.

ABSTRACT

In physics and engineering, abstract spaces composed of different system parameters allow visualizing fundamental laws and employing geometrical tricks. Here we discuss some examples for the study of imaging and nonimaging optical systems.

Keywords: Mappings, Poincaré sphere, geometry, OTF, reflectors

1. INTRODUCTION

The development of geometry and physics (and in particular, optics) have gone hand-in-hand over the centuries, and some of the most profound theoretical achievements are those that manage to reduce the description of a physical phenomenon in terms of geometry. In some cases, such geometric descriptions do not take place in the physical three-dimensional space, but in an abstract one. One example is that of a "phase space" composed of a combination of physical variables (spatial coordinates or time) and their canonical conjugates (momenta or frequency). In optics, phase-space representations can be used to describe light propagation both in the ray or wave domains (e.g., through the use of Wigner functions [1]) as a simple linear geometric transformation of phase space.

A second example of an abstract space is that of the Poincaré sphere [2], used to describe the polarization of paraxial light. Consider for example a purely monochromatic beam, where at each point the electric field vector traces over time an ellipse normal to the propagation direction, as shown on the left panel of Fig. 1. The orientation, ellipticity and handedness of this ellipse are the geometric properties that we call polarization. These can be described in terms of two angles: ϕ which determines orientation, and θ which determines ellipticity and whose sign determines handedness. The Poincaré sphere is the abstract spherical space in which these two angles correspond to longitude and latitude, respectively. Note that a useful abstract representation is not simply the consequence of mapping parameters to a given space: the shape of the space must be one that incorporates naturally the relevant physical transformations. For example, the action of phase retarding elements on a field corresponds to a rotation of the Poincaré sphere [2,3], and phenomena such as the geometric phase [3,4] have a simple geometric interpretation in terms of this abstract representation.

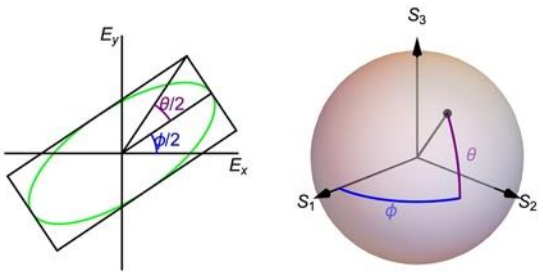

Figure 1. The Poincaré sphere, used commonly in the study of polarization, is a geometric representation of an ellipse with a given orientation, ellipticity, and handedness, as a point over the surface of a unit sphere.

*miguel.alonso@fresnel.fr; miguel.alonso.perso.centrale-marseille.fr

The work described in this manuscript presents recent examples in which abstract representations permit the use of geometry to describe (either exactly or approximately) the behavior of different types of optical systems.

2. MAPPINGS

A recurrent idea in the work presented in what follows is that of a mapping, which corresponds to a convention for transferring the coordinates of each point in one space to a point (or points) in another. For example, consider mapping a flat two-dimensional space with coordinates x and y to another flat two-dimensional space with coordinates x' and y'. One particularly useful type of mapping [5] results from considering x and y as the real and imaginary parts of a complex number, and x' and y' as the real and imaginary parts of an analytic function of $x + \mathrm{i}\, y$. This type of mapping is mapping is conformal, meaning that angles are preserved, with the exception of points where the derivative of the function is zero or singular. One particularly interesting example is that of the "square mapping" for which $x' + \mathrm{i}\, y' = (x + \mathrm{i}\, y)^2$, that is, $x' = x^2 - y^2$ and $y' = 2xy$. This mapping is illustrated in the first row of Fig. 2. Note that, because of the squaring, each half-plane of the original space is mapped onto the complete mapped space. Also, note that this mapping is conformal except at the origin. The second row of Fig. 2 shows the same mapping, but where the underlying grids are composed of lines of constant x' and y'. This is to illustrate that there is an inverse mapping, given by a square root, where each point maps onto two points.

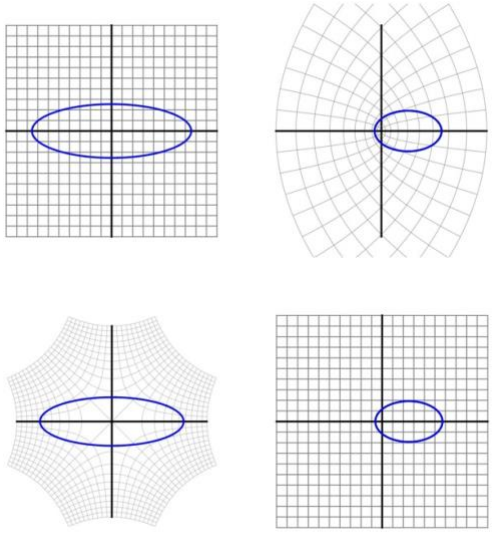

Figure 2. Square mapping, from x,y (left) to x',y' (right). The top row uses a grid of lines of constant x and y, while the second uses a grid of lines of constant x' and y'. Also shown is the mapping of an ellipse centered at the origin to an ellipse centered at a focus.

A remarkable aspect of the square mapping is that it maps conic sections centered at the origin onto other conic sections centered at a focus [6]. This is illustrated in Fig. 2 for the case of an ellipse. Physically, conic sections centered at the origin can be thought to correspond to the orbits of a particle in an isotropic quadratic potential: when the coefficient of the quadratic is positive, the potential is attractive and the orbit is an ellipse (which mathematically corresponds also to the path traced by a monochromatic electric field at a point, that is, to polarization); if on the other hand the potential is repulsive, the conic is a branch of a hyperbola centered at the crossing of its asymptotes; finally, if the coefficient of the quadratic is zero, the potential is constant and the trajectory is a straight line (corresponding to a free particle). On the other hand, the square mapping of these three types of curves gives conics that are centered at a focal point, which correspond to Keplerian orbits, respectively: a bound elliptical orbit (as shown in Fig. 2), a non-periodic hyperbolic orbit, and their boundary, an "escape" orbit of parabolic shape. As will be described in what follows, this mapping also has connections with the behavior of optical systems.

3. LASER CAVITIES WITH ABERRATIONS

Some of the ideas presented so far can be applied to the description of the type of optical cavities used in lasers, composed of a pair of curved mirrors, as shown in Fig. 3(a). The modes of such cavities can be described in terms of ray optics by considering a two-parameter family of rays that, following a round trip, keep the same configuration both in position and direction (even though each ray might cycle within such family at each trip). The phase space for describing the rays consists of two transverse coordinates (say, at the central plane of the cavity) of each ray, and its two transverse direction cosines. Each passage through the cavity is modeled as a linear operation on these four parameters, corresponding to a linear transformation in this four-dimensional phase space, which is difficult to visualize.

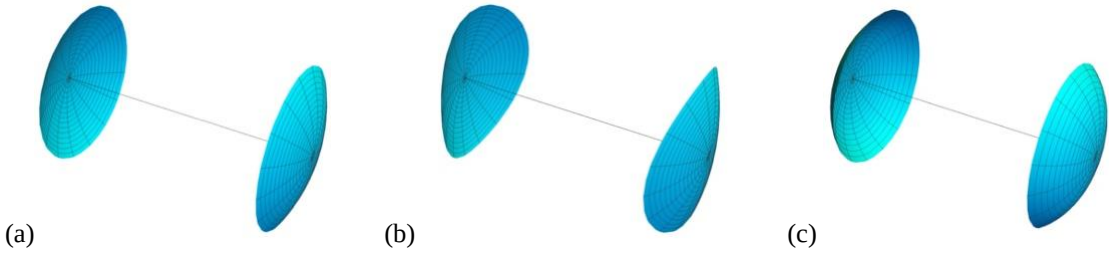

Figure 3. Optical cavities composed of two identical mirrors: a) without aberrations, b) with astigmatism, and c) with spherical aberration.

It turns out that it is possible to still provide a complete description of this system while reducing the dimensionality of the phase space used. The key is associating a point not with each ray, but with a one-parameter subset of the rays. Notice that, for a perfect cavity, there are families of rays like the bundle shown at the right panel of Fig. 4, which at any plane of constant z (the axial direction) has a cross-section that is elliptic, where the ellipse has the same ellipticity and orientation and only changes in size. Note also that the rays composing this bundle are skewed, and this skewness gives the ellipse a handedness. It is then possible to borrow the Poincaré sphere construction and represent this bundle (with given orientation, ellipticity and handedness) as a point over the surface of a sphere, as shown on the left panel of Fig. 4. To distinguish this sphere from that for polarization (where the axes are the normalized Stokes parameters), we use the symbol T_n to identify the axes. In this context, the Poincaré sphere is a reduced version of the phase space for the rays.

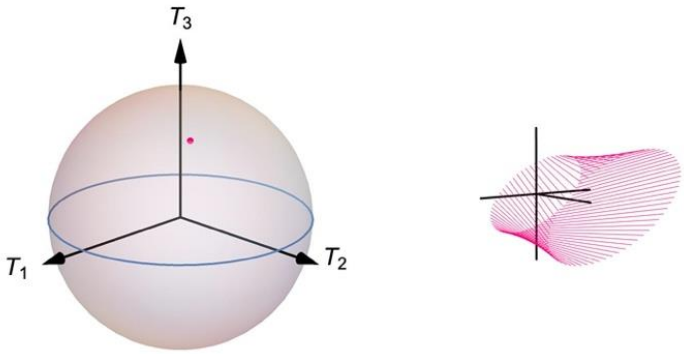

Figure 4. The Poincaré sphere construction used for characterizing a bundle of rays with elliptical cross section.

The complete set of rays for a mode constitutes a two-parameter family, i.e., a one-parameter set of these elliptical bundles, each of which is a point over the sphere. The mode is then given by a curve over the sphere, as shown in Fig. 5. The shape of the curve over the sphere fully encodes the geometry of the mode [7]. The standard modes, such as Hermite-Gaussian or Laguerre-Gaussian modes can be described in this way. Further, the possibility of transforming one type of mode to the other with combinations of cylindrical lenses can be modeled through ray tracing by using these ray families, and these transformations turn out to correspond simply to rotations of the sphere.

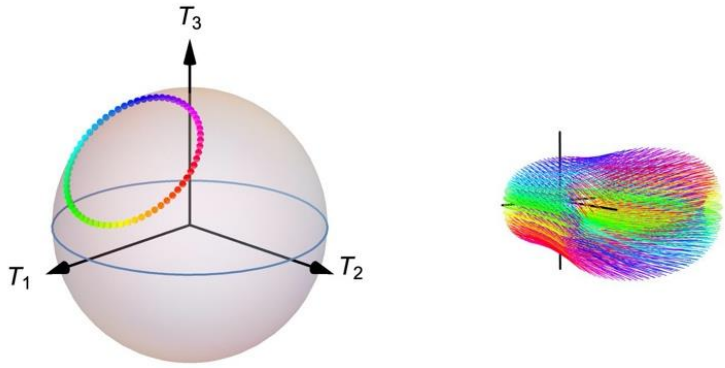

Figure 5. The rays associated with a mode on a cavity can be represented as a curve over the Poincaré sphere. Here, the different points along this curve are shown in different colors so they can be identified with the corresponding ellipses of rays on the right.

The most striking features of a beam often can be associated to the ray caustics [], which are the envelopes that contain them and at which the ray density is infinite. A remarkable geometrical relation exists between these caustics and the projection of the path over the Poincaré sphere onto the equatorial plane, which is described in detail in Ref. 7. For brevity we do not describe this relation here, but just mention that the square mapping described in Section 2 plays a central role in it. Further, the variables T_n over the Poincaré sphere can be associated to the action of small amounts of aberrations on the cavity mirrors [4]: astigmatism aligned with the *xy* axes (Fig. 3(b)) is related to T_1, astigmatism aligned at 45 degrees from the axes is related to T_2, and spherical aberration (Fig. 3(c)) is related to the square of T_3. This interpretation permits understanding the structure of other types of modes, such as the so-called Ince-Gaussian beams [9], and reveals the mathematical and geometrical analogy between fields in aberrated optical cavities and several very different physical systems ranging from the simple pendulum to cold atom clouds with nonlinear interactions according to the Bose-Hubbard dimer model [10].

4. FREEFORM REFLECTORS FOR NONIMAGING APPLICATIONS

The square mapping turns out to be useful also within a very different context: that of non-imaging optics in cases where the problem can be reduced to two dimensions [11]. Consider the problem of designing a reflector that redirects the light from a point source in order to achieve some desired far-field illumination pattern. To illustrate this idea, let us start with a simple case in which we want to send a specified amount of optical power in three directions at prescribed angles with respect to the horizontal. The proposed design method based on the square mapping is the following: i) draw three contiguous line segments (as shown in either of the panels on the left of Fig. 6), whose angles from the horizontal are half the angles at which the light must be directed, and where the angle subtended by each segment from the origin is proportional to the amount of power to be sent in the corresponding direction; ii) by simply applying the square map to this graph, one finds a shape for a reflector composed of three parabolic segments that achieves the desired goal [11]. The two examples in the top and bottom rows of Fig. 6 correspond to convergent and divergent reflector designs.

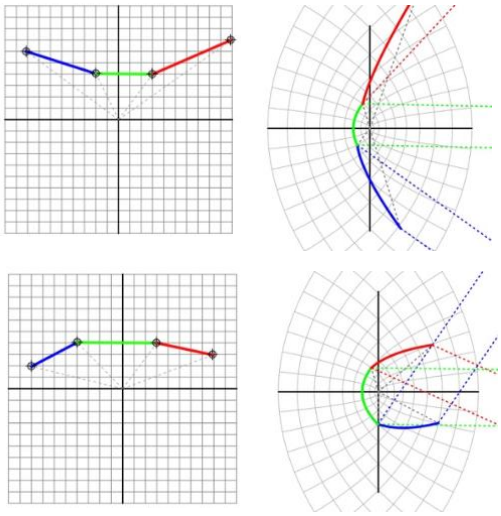

Figure 6. Left: light curves composed in this case of three straight segments. Right: the corresponding piecewise parabolic reflector shapes, given by the square mapping of the light curve. The angle from the horizontal of each segment of the light curve is half of that in which the reflector will redirect light, and the angle subtended by each segment from the origin is half of that subtended by the corresponding reflector segment. A light curve bent upwards (top) or downwards (bottom) indicates whether the reflector will be divergent (for which the rays do not cross) or convergent (for which the rays cross).

The key for this mapping process is the property of the square map of transforming straight lines (analogous to free trajectories) to parabolas (analogous to Keplerian escape orbits). While the examples just described are for piece-wise parabolic reflectors, one can apply these concepts to continuous reflectors by considering the limit. In fact, one can use the reverse mapping to start from a given reflector shape to find where the light will be directed. The inverse (or "square-root") mapping of a reflector gives what we referred to as a "light curve" which reveals not only where the light goes, but also whether segments of the reflector are converging (for which the light curve bends downwards) or diverging (for which the light curve bends upwards), and if there are far-field caustics (corresponding to inflection points of the light curve). Rigid shifts of a mirror cause deformations of the light curve, and this can be used to study the effects of misalignments or of extended sources (or targets). Many examples are provided in Ref. 11.

5. ABERRATIONS IN IMAGING SYSTEMS

Let us present one final example in which an abstract representation combined with geometry aids in the description of optical systems, in this case imaging systems. Consider a simple telecentric imaging system, as that shown schematically in Fig. 7, used to form images of a planar, spatially incoherent object. The Optical Transfer Function (OTF) is one of the standard measures of the imaging capabilities of a system. It describes how well (that is, with what contrast) the system can reproduce each spatial frequency component of the object.

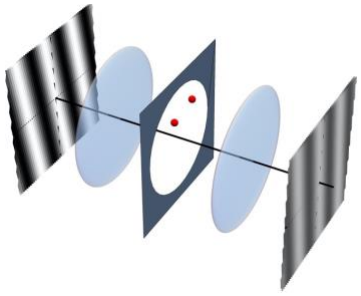

Figure 7. A representative imaging system with a circular pupil. The OTF determines the contrast at the image plane of each spatial frequency of the object (one of them shown in the figure).

The OTF is affected considerably by aberrations in the system. Let us assume, as is customary, that the aberrations are represented as wavefront errors at the plane of the pupil, assumed here to be circular and placed at a plane that is Fourier-conjugate to the object and image (due to telecentricity). The Pupil Difference Probability Density (PDPD) was defined recently [12-15] as a tool for characterizing this error. To understand its meaning, consider any two points within the circular pupil. The vector separation between these two points corresponds to a spatial frequency of the object or image: if two mutually coherent point sources were to be placed at these points, their interference fringes would have the corresponding spatial frequency. Clearly, there are many such pairs of points with the pupil with the same vector separation. The PDPD is defined as the probability density for the difference in aberration at any such two points with the prescribed vector separation. The arguments of the PDPD are then the vector separation between the points (which corresponds to a spatial frequency), and the aberration difference η, over which it is normalized to unity. For example, for an unaberrated system, the PDPD is a Dirac delta distribution in η. The usefulness of the PDPD relies on two properties: it can be calculated exactly or approximately for several types of aberration, and its 1D Fourier transform in η gives the ratio between the OTF as a function of aberration strength (in waves) and that of the corresponding aberration-free system.

The PDPD can be used to calculate useful analytic approximations for the OTF. Consider the simple case of a system with defocus, for which no closed form exists for the OTF. The PDPD for this case can be calculated exactly [14]: for a given spatial frequency (regardless of its direction given the rotational symmetry of the problem) the PDPD is zero outside of a given region, and inside this region it corresponds to the intersection of two elliptic segments, as shown on the left panel of Fig. 8. This function does not have a closed-form Fourier transform, explaining why there is no exact closed-form expression for the OTF. However, a very accurate approximation to the PDPD is given by the sum of an ellipse and a triangle distributions, as shown in Fig. 8, which when chosen correctly [14] match the PDPD to within 2%. These two distributions do have simple closed form Fourier transforms: a Bessel function of order 1 divided by its argument, and a sinc squared, respectively. This results in an accurate, simple expression for the OTF for defocus.

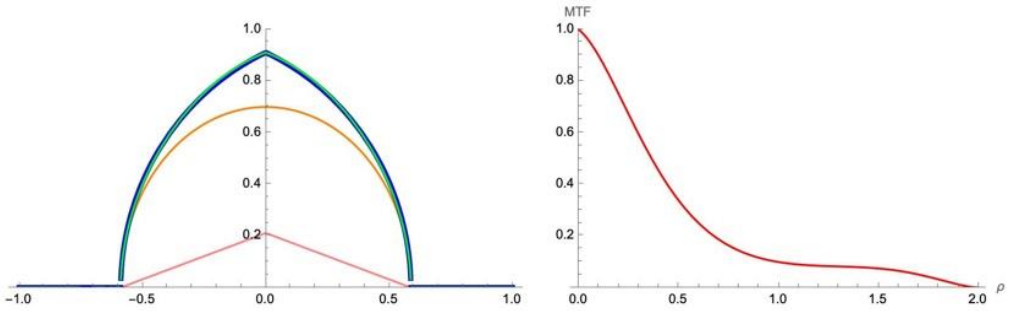

Figure 8. Left: PDPD (blue) at a given spatial frequency for defocus, and its approximation (green) given by the sum of an ellipse (yellow) and a triangle (red) distributions. Right, The resulting OTF estimate.

The same type of trick can be used for more complex aberrations, such as those resulting from the groove structure defects left behind in optical surfaces by milling and turning fabrication processes. It is shown in Ref. 7 that by working on the "abstract space" provided by the PDPD, performing mappings over the spatial frequency variables, and then using geometric approximations over the dependence in η, accurate analytic estimates can be found for the OTF of systems presenting these complex aberrations. The example of concentric grooves is illustrated in Fig. 9. The statistical nature of the treatment allows even incorporating the effects of random variations in the amplitude and periods of the grooves, caused by fluctuations in the thrust and feed of the fabrication process [15].

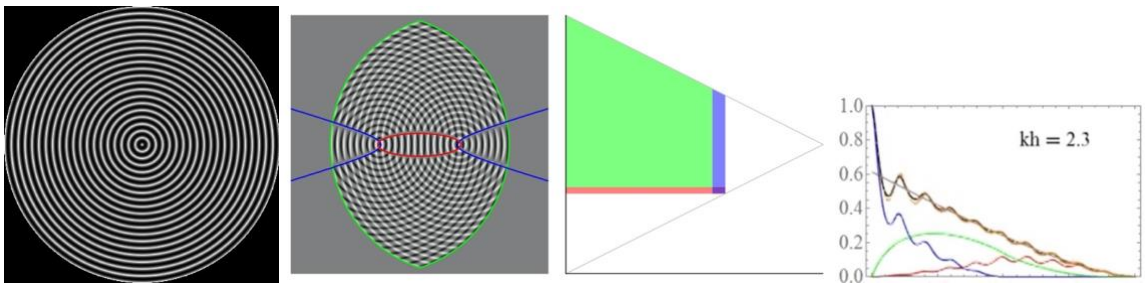

Figure 9. First from left: groove structure aberration caused by diamond milling manufacturing. Second from left: difference between two shifted versions of the aberration, whose probability density is the PDPD. Notice that the regions inside the blue hyperbolic contour and the red elliptic contour are those where the grooves of both replicas are roughly aligned. Third from left: A simple mapping transforms the regions inside the red ellipse, the blue hyperbola, and the rest, onto simple quadrilateral regions that facilitate the computation. Each of these regions gives a different type of contribution to the OTF. Fourth from left: analytic OTF estimate (black) as a function of spatial frequency, composed of the sum of the three contributions (blue, red, and green) compared to a rigorous numeric computation (orange), for the case where the height of the groove-shaped aberration is $2.3/2\pi$ waves.

6. CONCLUDING REMARKS

The study of many optical systems can be facilitated by introducing the appropriate abstract representation (such as a Poincaré sphere for rays in an optical cavity, the so-called "light-space" for illumination reflectors, or the PDPD for the study of optical systems) and applying mappings and other geometric analysis to arrive at a simplified description.

7. ACKNOWLEDGEMENTS

I would like to thank the coauthors of prior publications [3,7,10-15] on the topics described here; in alphabetical order: Luis Arturo Alemán-Castañeda, Mark R. Dennis, Greg W. Forbes, Rodrigo Gutiérrez-Cuevas, Kevin Liang, Duncan O'Dell, and Anthony Vella. I also acknowledge funding from the NSF's I/UCRC Center for Freeform Optics (IIP-1338877), and the Excellence Initiative of Aix-Marseille Université – A*MIDEX, a French "Investissement d'Avenir" programme.

REFERENCES

[1] Alonso, M. A., "Wigner functions in optics: describing beams as ray bundles and pulses as particle ensembles," Adv. Opt. Phot. **3**(4), 272-365 (2011).
[2] Born, M. and Wolf, E., [Principles of Optics: Electromagnetic Theory of Propagation, Interference and Diffraction of Light], Cambridge University Press, Cambridge, 7th Edition, 32, (2000).
[3] Vella, A. and Alonso, M. A., "Poincaré sphere representation for spatially varying birefringence," Opt. Lett. **43**(3), 379-382 (2018).
[4] Bliokh, K. Y., Alonso, M. A., and Dennis, M. R., "Geometric phases in 2D and 3D polarized fields: geometrical, dynamical, and topological aspects," Rep. Prog. Phys. **82**(12), 122401 (2019).
[5] Brown, J. and Churchill, R. [Complex Variables and Applications], McGraw-Hill, New York, 372-399 (2009).
[6] Needham, T, "Newton and the Transmutation of Force," Am. Math. Month. **100**(2), 119-137 (1993).
[7] Alonso, M. A. and Dennis, M. R., "Ray-optical Poincaré sphere for structured Gaussian beams," Optica **4**(4), 476-486 (2017).
[8] Nye, J. F., [Natural Focusing and Fine Structure of Light: Caustics and Wave Dislocations], Institute of Physics Publishing, Bristol, 1st Edition (1999).
[9] Bandres, M. A. and Gutiérrez-Vega, J. C., "Ince-Gauss beams," Opt. Lett. **29**(2), 144-146 (2004).
[10] Gutiérrez-Cuevas, R., O'Dell, D. H. J., Dennis, M. R., and Alonso, M. A., "Emulating a many-body topological transition with an aberrated optical cavity," arXiv 2106.02712 [physucs.optics], (2021).

[11] Alemán-Castañeda, L. A. and Alonso, M. A., "Study of reflectors for illumination via conformal maps," Opt. Lett. **44**(15), 3809-3812 (2019).
[12] Alonso, M. A. and Forbes, G. W., "Strehl ratio as the Fourier transform of a probability density of error differences," Opt. Lett. **41**(16), 3735-3738 (2016).
[13] Liang, K., and Alonso, M. A., "Understanding the effects of groove structures on the MTF," Opt. Express **25**(16), 18827-18841 (2017).
[14] Liang, K., and Alonso, M. A., "Effects of defocus and other quadratic errors on OTF," Opt. Lett. **42**(24), 5254-5257 (2017).
[15] Liang, K., and Alonso, M. A., "Effects on the OTF of MSF structures with random variations," Opt. Express **27**(24), 34665-34680 (2019).